Stage-1 phases of alkali-metal-doped conducting polymers

Dong Chen and M. J. Winokur
Department of Physics, University of Wisconsin, Madison, Wisconsin 53706

Yong Cao and A. J. Heeger
Department of Physics, University of California, Santa Barbara, California 93106

Frank E. Karasz
Department of Polymer Science and Engineering, University of Massachusetts, Amherst, Massachusetts 01003
(Received 29 April 1991)

The stage-1 phases of both Rb-doped *trans*-polyacetylene (PA) and Cs-doped poly(*p*-phenylene vinylene) (PPV) have been investigated by *in situ* x-ray diffraction, using highly oriented vapor-doped samples. While the relative guest-host sizes are nearly equivalent, the resulting equatorial structures, as determined by structure-factor calculations, exhibit pronounced differences in the location and orientation of the polymer chains. PPV samples are dominated by uniform chain-axis rotations within a base-centered orthorhombic lattice of the Cs^+ ions while PA undergoes displacive translations within a centered tetragonal lattice of the Rb^+ ions. Significant differences in the dopant-ion organization within the quasi-one-dimensional alkali-metal ion channels are also found. These temperature insensitive and polymer specific variations are indicative of local guest-host interactions which stabilize the respective structures. Further comparisons suggest that in PA systematic intermediate-length-scale deviations from planarity by the polymer chains are probable. As a result, the electronic excitations may couple to polymeric torsional degrees of freedom.

I. INTRODUCTION

The doped phases of conducting polymers have been studied extensively, primarily, for the unusual one-dimensional electronic excitations exhibited[1-3] and, more recently, because they also are representative of low-dimensional guest-host systems with strongly anisotropic interactions.[4-6] Initial structural studies, using both direct[7-9] and indirect methods,[10] were mainly focused on identification of the basic doping-induced symmetries and their structural motifs. More recent work,[11-14] using improved materials and *in situ* techniques, has begun to elucidate the full range of structural behavior associated with these low-dimensional complexes.

The subtle competition of forces between the chains of the polymer host and those of the dopant ions give rise to a variety of structure phases and phase transformations. Further insight into the nature of these interactions may be obtained by examining the structural variations as function of temperature[15] and/or pressure.[16] As the microscopic nature of these materials becomes better understood, it should be possible to develop a more complete picture of the size-scaling relationships.[17] In addition, continued structural refinements should enable more precise theoretical treatments that address the three-dimensional aspects of the overall conduction process.[2,18] Alkali-metal-doped derivatives are particularly well suited for detailed structural studies because there are minimal disruptions to the integrity of the guest-host matrix[19] upon doping. With larger molecular dopants there is often a significant loss in the quality of the scattering information available.[20] In addition, alkali-metal-doped samples are extremely stable when rigorously maintained in a nonoxidizing environment.

The simplest "family" of conducting polymers studied, so far, are the linear unsubstituted compounds comprised of only carbon and hydrogen. These include polyacetylene (PA), poly(*p*-phenylene vinylene) (PPV), and poly(*p*-phenylene) (PPP) [shown in Fig. 1(a)]. In their pristine state, all of these compounds are essentially one-dimensional semiconductors with direct band gaps of approximately 1.4 eV, 2.5 eV, and 3.0 eV, respectively. Both PA and PPV samples can be processed into robust high-strength films and, in the case of PPV, with good ambient stability. As is well known, the doping-induced structural changes are accompanied by profound changes in the optical and electronic properties.[21] Regardless of alkali-metal-dopant concentrations PA films always appear silvery but in PPV, there is a dramatic visual change from a translucent yellow to a silver or golden luster. Currently the highest recorded conductivities exceed 10^5 $\Omega^{-1}\,cm^{-1}$ and 10^4 $\Omega^{-1}\,cm^{-1}$ in doped PA (Refs. 22 and 23) and PPV (Ref. 24) compounds, respectively. While such values are common to conventional metals, these conducting polymers do not behave as simple metals for there is still pronounced infrared absorption in heavily doped materials.[25] Heavily doped conducting polymers also exhibit a measurable conductivity drop at reduced temperatures[26] but much of this response can be attributed to their specific morphological construction.[27]

On a microscopic level all three host materials may be considered, to first order, as representative of anisotropic extended rods.[6] Polycrystalline films of these materials are dominated by tightly packed formations in which the

individual chains bundle together with considerable regularity so that their projected cross sections, orthogonal to the polymer chain axis, exhibit $p2gg$ symmetry[28,29] [see Fig. 1(b)]. In this configuration there is strong bonding along the polymer backbone and considerably weaker interchain interactions. As a direct consequence of this pronounced anisotropy, dopant-ion interdiffusion into the host matrix induces both rotational and translational motions of the polymer chains. This behavior contrasts to the doping process of the quasi-two-dimensional layered intercalation compounds which undergo dilation as the primary response to dopant uptake.

For small, spherically symmetric dopants (e.g., the alkali metals), transformations into quasi-one-dimensional alkali-metal-ion channel structures dominate. The smallest alkali-metal-ions (Li[30] and Na[11,31]) primarily induce polymer-host chain rotations to form threefold channel structures wherein linear arrays of dopant ions are surrounded by three polymer chains. Doping by larger alkalis involves both rotational and translational displacements to yield fourfold channel structures with alkali-metal-ion galleries that are enriched by four polymer chains. These latter compounds also exhibit pronounced three-dimensional interchannel dopant-ion correlations.[32] Nominally, the threefold to fourfold crossover is sensitive to the relative counter-ion/polymer-host size ratios[17] for only Cs-doped PPV (PPV being somewhat larger than PA) has a fourfold channel structure whereas K-, Rb-, and Cs-doped PA all undergo a transformation to a fourfold structure.

Additionally, there is now clear evidence for the existence of subtler structural features, such as chain-axis rotations in the case of Cs-doped PPV and chain-axis displacements in alkali-metal PA samples, that alter the nominal stage-1 structure (001) projection depicted in Fig. 2(a). For stage-1 K-doped PA, the polymer chains translate along their major axis to yield the lower symmetry $P2gm$ structure shown in Fig. 2(b).[12] This modification of the original unit cell is directly inferred by the presence of a symmetry forbidden reflection in the scattering profiles. Other possible structural distortions have been forwarded,[14,33,34] but the actual magnitude and direction of these displacements are not reported. In stage-1 Cs-doped PPV, rotations of the polymer chains about the chain axis are dominant [as shown in Fig. 2(c)]. This distortion does not alter the $P4mm$ symmetry of the basic model in Fig. 2(a). Hence, no new reflections are observed, but the predicted intensities of the existing peaks are strongly modified.

In this paper we present results of an *in situ* vapor doping study of stretch-oriented Rb-doped PA and Cs-doped PPV. Direct comparison between these two materials is

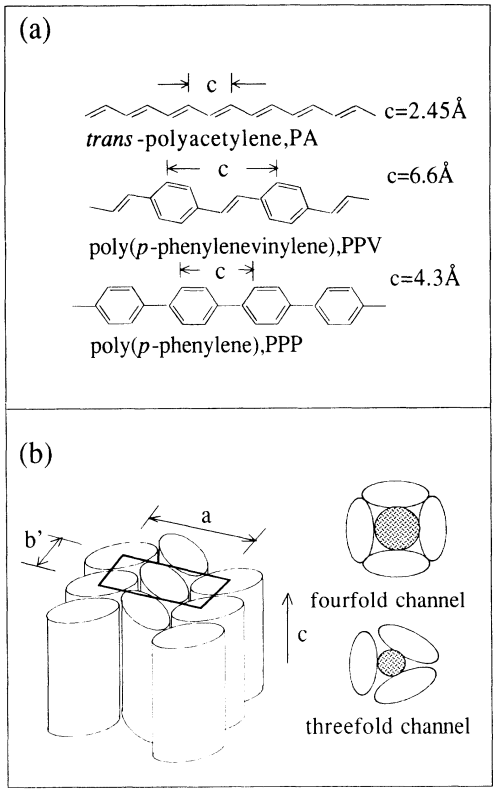

FIG. 1. (a) Projected c-axis structures of three prototypical conjugated polymers. (b) Packing of polymer chains when undoped (on left) and after alkali doping to threefold and fourfold channel structures.

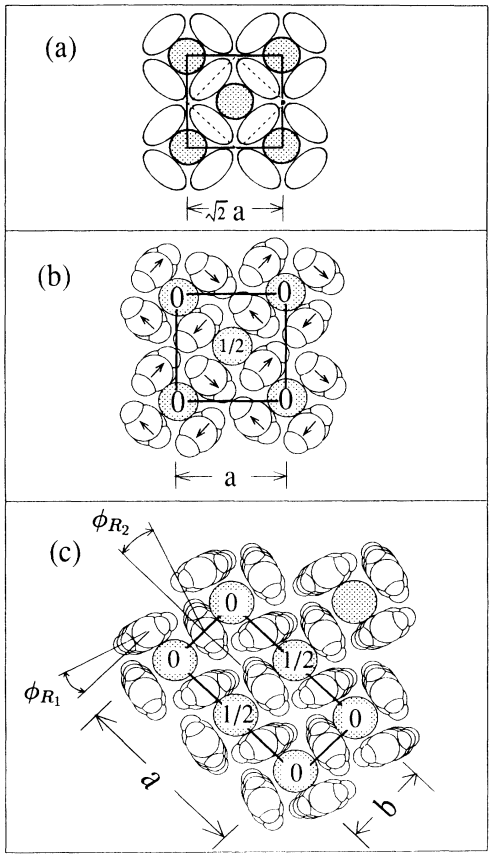

FIG. 2. Projected equatorial structure (perpendicular to the c axis) for (a) nominal $p4mm$ symmetry of stage-1 alkali-metal-doped polymers; (b) stage-1 alkali-metal-doped PA; (c) stage-1 Cs-doped PPV.

especially interesting for their relative projected two-dimensional (2D) guest-host sizes are very nearly the same. Thus, similarities and differences may be assessed more comprehensively and the unique response of each, due to the variations in the chemical nature, can be highlighted. We find that the lateral displacement which characterizes the polymer chains in stage-1 K-doped PA is also unambiguously present in stage-1 Rb-doped PA. Hence this response must be intimately related to the specific details of the local chain-ion interactions. As previously reported[12] Cs-doped PPV is dominated by chain-axis rotations that effectively reduce the minimum polymer chain to dopant-ion spacing. In addition, we find strong evidence for the presence of a lower 2D symmetry in the basal-plane projection for the Cs-doped PPV compounds. In this paper the thermal response of these structures has also been examined and analyzed by using comparisons with structure-factor calculations. In either case, the fundamental displacements and respective equatorial structures are found to be essentially temperature insensitive.

By using highly oriented materials, the nonequatorial structure has also been investigated. As is now well known, the alkali-metal ions in stage-1 PA compounds exhibit a centered tetragonal[32,33,35] packing with considerable interchannel axial disorder. In contrast, analysis of the nonequatorial scattering data for stage-1 Cs-doped PPV reveals that a base-centered orthorhombic lattice is more satisfactory. Both structures are characterized by a slight sensitivity to temperature with only modest losses in the interchannel alkali-metal-ion ordering at elevated temperatures. In agreement with previous reports, we find that both stage-1 structures exhibit incommensurability between the alkali-metal-ion axial repeats and those of the surrounding polymer chains. For Rb-doped PA, analysis of this nonequatorial data allows us to estimate the magnitude of the alkali-metal-ion displacements parallel to the channel axis.

These basic structures notwithstanding, there are other pronounced differences between the channel structures of the PA compounds and those of PPV. For Rb-doped PA, the intrachannel alkali-alkali coherence length, ξ_{Rb}, is ≈ 25 Å, similar to that of K- and Cs-doped PA,[36] whereas ξ_{Cs} in stage-1 Cs-PPV is typically over 70 Å. This intrachannel organization is essentially temperature independent except for a systematic increase in the alkali-metal-ion root-mean-square displacements at elevated temperatures. To explain this anomalously small ξ in PA, we theorize that there are intermediate-length-scale distortions along the polymer chain axis that lead to pronounced polymer chain twists and isolate the alkali-metal ions within shorter axial domains.

II. EXPERIMENTAL DETAILS

Thin PPV films (typically 10 μm thick) were obtained by thermal conversion of a precursor polymer[37] poly(*p*-xylene-α-dimethylhydrothiophenium chloride) which was simultaneously processed in a uniaxial web stretching device[38] to final draw ratios of $\approx 10{:}1$. Uniaxial stretching tends to orient the *c* axis (or polymer chain axis) parallel to the draw direction and these highly oriented polymer films exhibited *c*-axis mosaic spreads of typically less than 10° [as determined by measuring equatorial ($hk0$) angular widths at half maximum]. After the conversion process, the PPV films were annealed under dynamic vacuum at 300 °C (ca. 4 h) to improve their crystallinity.[39,40] For these undoped films, the coherence lengths were found to be ≈ 150 Å along the *c* axis and ≈ 110 Å in the lateral direction.[41]

Thin *cis*-PA films (typically 30 μm thick) were obtained by a modified Shirakawa method[42] and then uniaxial stretching in a home-built stretching device to draw ratios approaching 15:1. Prior to doping, the films were converted to an all-*trans* conformation by thermal annealing at 150 °C for ca. 1 h. These films also exhibited *c*-axis mosaics of less than 10° and coherence lengths exceeding ≈ 140 Å along the *c* axis and of ≈ 80 Å in the equatorial direction.

The polymer samples were carefully cut and clamped (or folded) so as to maintain the preferential orientation until dimensions of approximately $3.0\times1.5\times0.1$ mm^3 and $3.0\times1.5\times0.03$ mm^3 were reached for PA and PPV, respectively. All films were then transferred to x-ray glass capillaries into which a small quantity of alkali metal had been added. These cells were then sealed and mounted in a beryllium windowed furnace that attached directly to the x-ray diffractometer. For heavily Cs-doped PPV samples, modest attenuation of the transmitted x-ray intensities was experienced (due to absorption effects). The thin walls of the glass cell, typically 10 μm, minimized the parasitic glass scattering and maximized the x-ray transmission. To prevent structural failure, each glass cell required a partial pressure of Ar (≤ 1 atm). PA samples were heated to ~ 220 °C while PPV samples were doped at temperatures ranging from 240 to 270 °C. A two-zone furnace was employed, but alkali-metal source temperatures close to those for the polymer samples were necessary to ensure reasonable doping times. Although vapor doping avoids many complications of solvent-based doping techniques, we find this method affords only limited overall control of the doping process.[43] However, these *in situ* cells were extremely advantageous for the doping process could be monitored and then halted when the desired composition was reached. At no time was scattering from condensed alkali metal detected.

To perform elevated temperature studies, the samples were maintained in their doping cells. Once a saturated stage-1 Rb-doped PA sample was prepared, the structure was found to be very stable at temperatures below 200 °C. Extended high-temperature annealing did generate some slight Rb-hydride residues.[14] Cs-doped PPV was particularly troublesome in that the stage-1 structure does not represent the most heavily doped phase. Hence, nonequatorial studies at higher temperatures were complicated by continual doping and a slow evolution towards a saturation phase.[44] For reduced temperature measurements, a PPV doping cell was transferred to the cold finger of a closed-cycle He cryostat. The thin-wall glass cells were found to be sufficiently robust to withstand vacuum applications.

All structural studies employed a computer controlled four-circle diffractometer that was attached to a rotating-anode x-ray generator fitted with a copper target ($\lambda_{K\alpha}=1.541$ Å) and a bent-graphite monochromator. The cross-sectional area of the incident x-ray beam at the scattering center was set to $\approx 1.5\times 1.5$ mm^2. The scattered x rays were incident on a small, one-dimensional position-sensitive detector consisting of a refrigerated silicon diode array (EG&G PARC Model 1412XR) and associated electronics. The detector's spatial resolution was set by forming 16 pixel groups from the detector's 960 accessible 25 μm$\times$2 mm pixels. This diode array was located $\sim$30 cm from the scattering center and subtended a 2θ arc of $\sim$4.5°. Typical counting rates, for a single group at the most intense reflection of 100-μm-thick multilayer samples, were in excess of 50 counts per second per 16 pixel group. In order to minimize nonlinearities across the detector, a correction factor for each group was included and the 2θ step sized for each individual data collection point was limited to 0.5°. Because a linear detector images the curved arcs of the Ewald sphere, some distortion (at the detector ends) is introduced into the radial θ-2θ scans for oriented samples. Since the diode array has an angular resolution of only 4.5° and, since these polymers have a larger mosaic spread, this distortion is negligible.

In all cases, radial θ-2θ scans were performed. Equatorial scans maintain the scattering vector in a plane perpendicular to that of the polymer chain axis (or c axis) thus probing the cylindrically averaged ($hk0$) reciprocal lattice plane. For meridional scans the scattering vector is kept parallel to the polymer chain axis. Scans along directions intermediate to these two extremes were also performed.

III. EQUATORIAL STRUCTURE

As a result of the *in situ* methodology, dopant-ion uptake was directly verified by continually monitoring the equatorial diffraction profiles. Upon Rb doping, PA was found to transform into a stage-1 tetragonal phase via a disordered phase. This intermediate doping structure was inferred by an initial loss of undoped polymer scattering intensity and, concomitantly, an increase in scattering from a very broad feature centered at $2\theta\approx 18°$. This increased intensity is clearly evident in the second scan from the top in Fig. 3 (and marked by an arrow) in which the top profile has been translated downward for close comparison. Only after a portion of the PA host had transformed into this intermediate phase could scattering from the tetragonal phase be discerned. In the case of Cs-doped PPV, initial doping was marked by only the appearance of the stage-1 structure. Since PPV is noted for its poor doping characteristics, this result may only be indicative of a narrow boundary layer between undoped and stage-1 regions of the films. For both host compounds studied in this investigation, there is no evidence of higher-stage formation (at least at temperatures above 200 °C) at even the lightest alkali-metal doping levels as observed in other vapor-doped PA samples.[14,34] These results are, however, consistent with additional

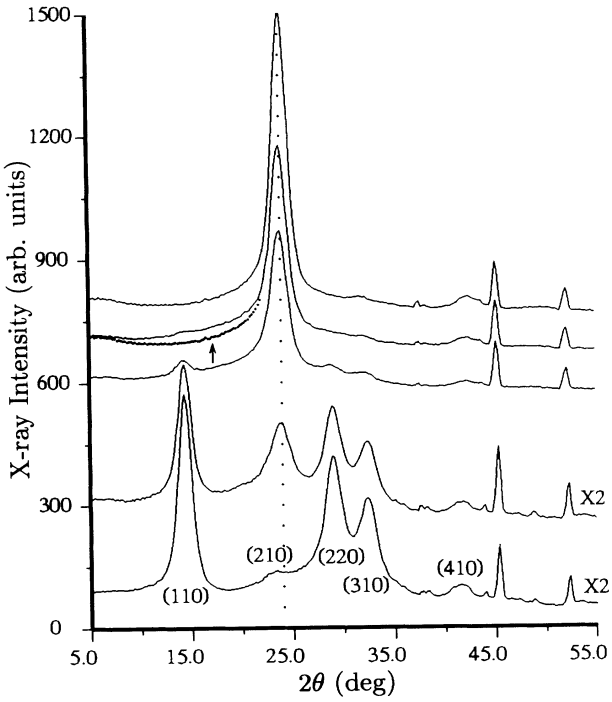

FIG. 3. Experimental equatorial ($hk0$) scattering profiles at the onset of rubidium doping (top three scans) and at the very end of the doping transition (bottom two scans) for a PA sample. The dotted profile, marked by an arrow, is the undoped PA curve shifted so that the scattering from an intermediate phase can be discerned. Sharp features near $2\theta=45.5°$ and $2\theta=52.5°$ are due to Be-window scattering.

claims of poor high-stage formation during the initial doping transition.[10,45]

The most important aspect of this technique was that the doping process could be observed at (or near) completion. For K-, Rb-, and Cs-doped polyacetylene, all previous reports of a lower-symmetry stage-1 structure have relied on the observation of a symmetry forbidden $(210)_{\text{St. 1 Rb(PA)}}$ equatorial peak in close proximity to scattering arising from to the most intense reflections of the undoped polymer host [a PA(020)+(110) superposition], and hence have been the subject of dispute. In our case, we can unambiguously identify this feature, labeled as the (210) reflection in Fig. 3, as intrinsic to the stage-1 structure of Rb-doped PPV. Rb-doped PA is particularly well suited for monitoring this reflection because the relative guest-host structure-factor contributions nearly cancel for the neighboring $(200)_{\text{St. 1 Rb(PA)}}$ reflection.[9]

Structure-factor calculations[43] that combine scattering from the undoped polymer, a heavily doped stage-1 structure, and a background contribution suggest that complete doping occurs and that this peak can only be interpreted as PA chain translations which are identical to the structural distortion reported for K-doped PA. For Rb-doped PA, the polymer chain-axis center of mass is displaced by 0.31 ± 0.05 Å along the polymer major-axis direction. No other displacements were found that yielded as satisfactory results. Because the structure-factor calculations are dominated by rubidium and carbon con-

tributions and since the PA carbon atoms are displaced by only 0.36 Å from the polymer chain-axis center, a direct confirmation of small PA chain rotations was not possible.

The observation of a translational displacement, essentially equivalent to that reported for K-doped PA, is extremely important for identifying its physical origin. Naively, a simple size-scaling argument could be forwarded as the most pertinent parameter. Since substantially different systems, Rb- and K-doped PA, experience identical distortions, it is apparent that the local nature of the ion-chain interactions is central to this displacement.

As the three equatorial scans in Fig. 4 show, structure-factor calculations achieve excellent fits at all three temperatures investigated, 300, 400, and 490 K. The best fits for this sample occur at calculated Rb concentrations of 16.0%, 15.7%, and 16.5% mole weight, respectively, values close to the 15.6% mole weight as indicated by the average 3.95 Å intrachannel ion-ion spacing measured directly (discussed in the next section), or compositions reported elsewhere using weight uptake or elemental analysis.[46] All three fits yield an essentially unchanging value for the translational displacement of the polymer chain axes. The equatorial temperature coefficient, B, using an exponential factor, $\exp(-B\sin^2\theta/\lambda^2)$, where $B=8\pi^2\langle\bar{\mu}^2\rangle$ and $\langle\bar{\mu}^2\rangle$ is an isotropic equatorial mean-square displacement, is relatively temperature insensitive. The only measurable systematic change was in the measured equatorial lattice constant. These results and those for the undoped polymer are summarized in Table I. In addition to these observations, measurable broadening of the equatorial reflections at higher angles did occur but with no clear evidence of splitting (indicative of a lower-symmetry structure). Hence, various types of disorder effects and/or unit-cell distortions are all reasonable explanations.[47]

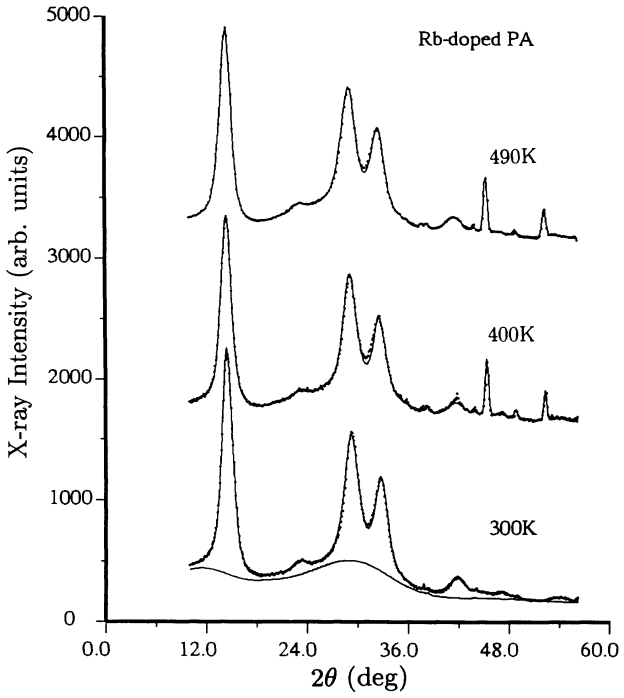

FIG. 4. Experimental data (dots) and calculated profiles (solid line) of equatorial ($hk0$) scattering at selected temperatures for a stage-1 Rb-doped PA sample. Sharp scattering features are artifacts (e.g., Be and salt residues). The curve at bottom is a representative background profile.

Cs-doped PPV, which has nearly the same guest-host size ratio as Rb-doped PA, manifests an alternate response with simple rotations of the chains axis about their center of mass. As the three profiles in Fig. 5 show, equatorial structure-factor calculations again achieve good agreement with the experimental data. Close inspection of the equatorial peak profiles combined with a

TABLE I. Lattice parameters as determined from structure-factor calculation for doped and undoped samples.

Sample	Temp. (K)	Lattice parameters a (Å)	b (Å)	Chain distortion shift (Å)		Temperature coefficient B (Å^2)
Stage-1	300	8.630		0.31		0.21
Rb(PA)	400	8.664		0.31		0.24
	490	8.707		0.32		0.23
Undoped	300	7.14	4.22			0.15
PA	490	7.26	4.22			0.17
				ϕ_{R_1} (deg)	ϕ_{R_1} (deg)	
Stage-1	20	13.49	6.85	25.0	26.5	0.23
Cs(PPV)	300	13.54	6.88	25.5	26.5	0.28
	540	13.78	6.99	25.6	28.4	0.32
Undoped	20	7.83	4.96			
PPV	300	7.93	5.03			0.20
	500	8.10	5.14			0.27

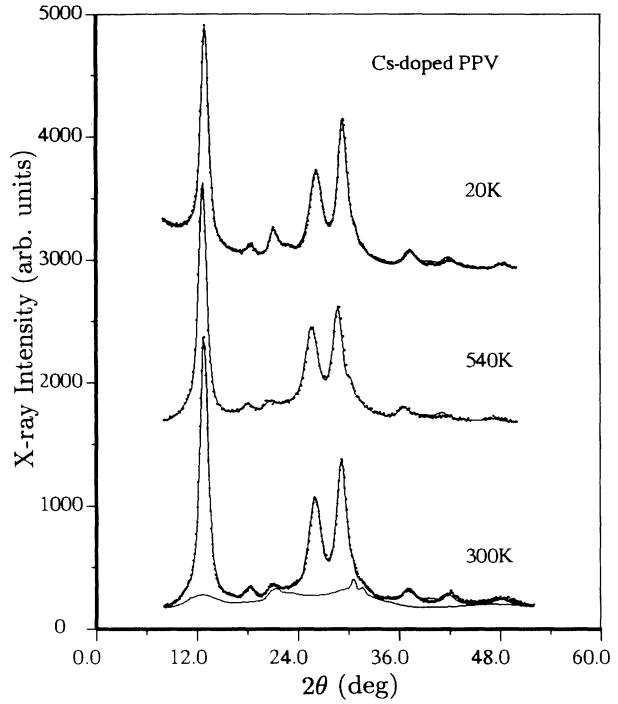

FIG. 5. Experimental data (dots) and calculated profiles (solid lines) of equatorial ($hk0$) scattering at selected temperatures for a stage-1 Cs-doped PPV sample. The curve at bottom is a representative background profile.

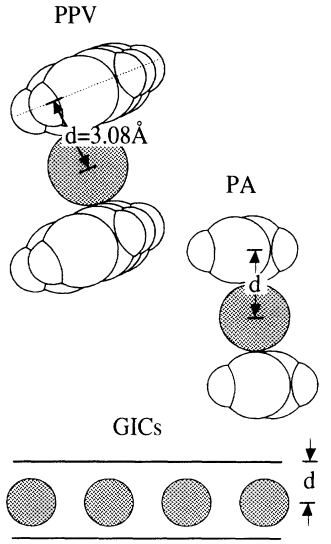

FIG. 6. Various guest-host spacings for Cs-doped PPV (on top), Rb-doped PA (middle), and stage-1 GIC (bottom) (Ref. 56) referred to in Table II and in the text.

peak-width analysis reveals features indicative of a rectangular 2D symmetry. The most obvious indication is in the anomalous broadening of the peak located at $2\theta=26.3°$ in comparison to the other peaks. This behavior was observed in all samples studied. For the sample shown in Fig. 5, the peak located at $2\theta=26.3°$ [a (400),(020) superposition] has a full width at half maximum of 0.11 $Å^{-1}$, while the widths of the reflections at $2\theta=18.5°$ and at 29.4° are 0.07 $Å^{-1}$, 0.08 $Å^{-1}$, respectively. This broadening can be reproduced in the calculated profiles by introducing the slight distortion of either $\mathbf{a}=1.97\mathbf{b}$ or $\mathbf{a}=2.03\mathbf{b}$ [see Fig. 2(c)]. Of the two possibilities, the former expression is considered more physical in light of the observation that neighboring Cs ions along the a axis are staggered (as discussed in the next section).

At room temperature, our best-fit results for this sample indicate a Cs-dopant concentration of 77% mole weight. This is very close to the 73% mole weight value suggested by the 4.5 Å repeat determined directly and is considerably better than an initial estimate.[17] For stage-1 Cs-doped PPV, temperatures as low as 20 K were probed. Even at 20 K, the equatorial temperature coefficient, B, remains moderately large indicating the presence of considerable static disorder. There are thermally induced variations in both the equatorial lattice constants and in the isotropic equatorial temperature coefficient. These results are also summarized in Table I. Interestingly, in Cs-doped PPV the thermal expansion is approximately a factor of 2 less temperature sensitive than for the undoped host.

Because of the rectangular symmetry of basic 2D unit cell, two chain-axis rotation angles have been included [see Fig. 2(c)] with rotations of $25.0(\pm0.5)°$ and $26.5(\pm0.5)°$ for ϕ_{R_1} and ϕ_{R_2}, respectively.[48] In principle, we cannot distinguish between the structure shown and one which incorporates alternating phenyl-ring rotations of both positive and negative angles. This latter structure is thought to be highly unlikely as the charge-transfer process induces appreciable double-bond character to the vinyl-phenyl carbon linkage and would severely reduce the likelihood of large-scale angular displacements over short distances. As Table I shows, the PPV chain rotation angles are only slightly temperature sensitive with modest increases of ~1.5° at 540 K and thus maintaining a fairly constant perpendicular chain major axis to channel-center distancing, **d**, of 3.08±0.02 Å, as shown at top in Fig. 6. We also find that this Cs-doped PPV structure is exceptionally well packed for the net equatorial dilation is by only ~15% during the transformation to the stage-1 structure. Significantly, both compounds appear to be dominated by strong chain-ion interactions which render their respective equatorial structural distortions temperature insensitive.

IV. NONEQUATORIAL STRUCTURE

By executing a series θ-2θ scans at varying angles of inclination from the equatorial plane to the c axis and then reconstructing a map of constant scattering intensity contours, a single plane of the reciprocal lattice could be imaged (without the distortion intrinsic to flat-flat photographs). This data is shown in Fig. 7(a) for a stage-1 Rb-doped sample at room temperature. Scattering profiles from one-dimensional arrays of atoms is characterized by parallel sheets of scattering.[49] In this projection, the $l=1$ and $l=2$ layer lines from linear Rb^+-ion arrays are clearly resolved. The perpendicular spacing of these layer

lines implies an average Rb-ion spacing of 3.95 Å within each column, close to the values previously reported.[50] Since the projected c-axis C-C spacing is 1.23 Å, the alkali-metal-ion repeat is incommensurate to that of the channel forming host.[14,36] Although we do not clearly resolve any intensity along the equivalent ($hk1$) layer line which would arise from scattering by the PA chains, data from stage-1 K-doped PA samples suggest that 3D ordering of the polymer host does occur.[51]

Intensity variations along the individual alkali-metal layer lines are indicative of interchannel ion-ion correlations and these intensity variations can be indexed by invoking a body-centered tetragonal packing of the alkali-metal ions. Thus, alkali-metal ions residing in adjacent nearest-neighbor columns are shifted on average by ± 1.97 Å (or $c_{Rb}/2$). Meridional scans (parallel to the polymer chain axis) yield similar profiles for the $l=1$ and $l=2$ layer lines. By measuring the leading edge half width half maximum of the $l=1$ layer line along the c axis, the alkali-metal-interchannel correlation length is estimated to be only 25 Å. While this is similar to that seen in K- and Cs-doped PA,[36] it is dramatically less than the ~100-Å c-axis correlation length of the surrounding polymer chains and it also implies a loss of coherence over an interval of only six dopant ions.

By summing scans which do not contain ($hk0$) equatorial scattering, the nonequatorial scattering for a "powder" sample is approximated. Data for three different temperatures are shown at bottom in Fig. 8 and the Rb^+-ion scattering gives very broad profiles that completely dominate these diffraction spectra. On heating, the most pronounced features at ~26° and ~32° [essentially the (101) and (211) reflections, respectively, for stage-1 Rb-doped PA] appear to broaden slightly and

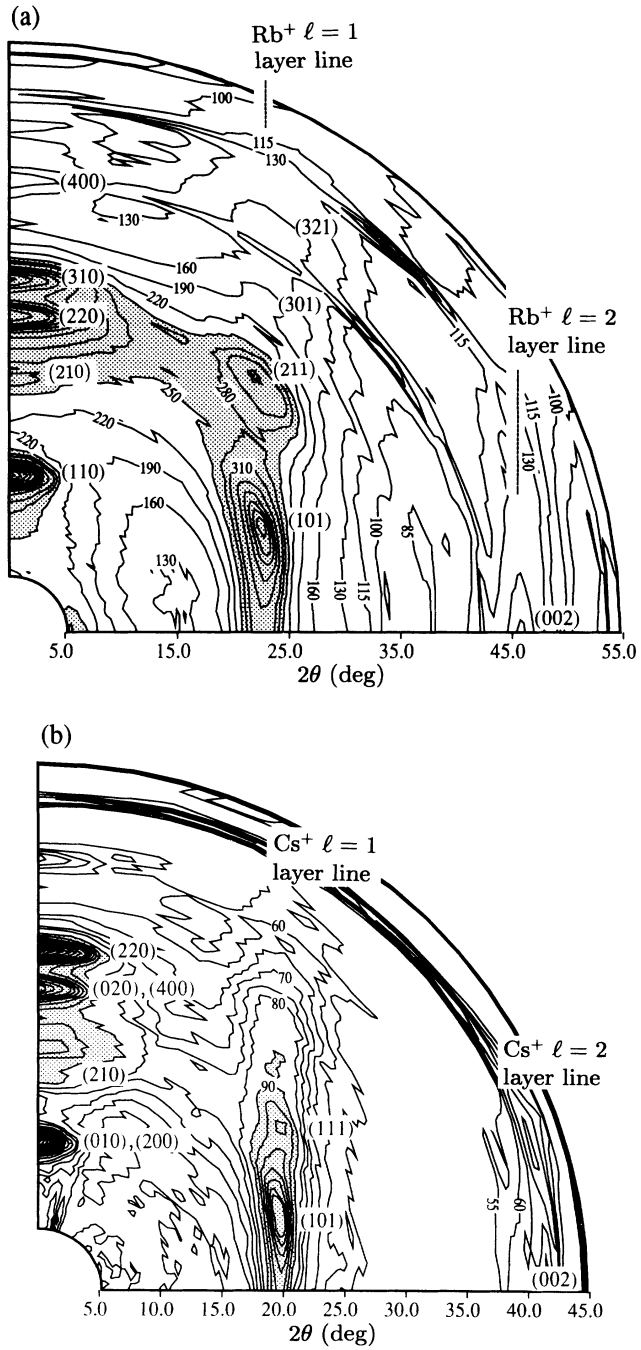

FIG. 7. (a) Map of the constant-scattering-density contours from the equatorial ($hk0$) plane to the c axis (parallel to the polymer chain axis) for a stage-1 Rb-doped PA sample. (b) Map of the constant-scattering-intensity contours from the equatorial ($hk0$) plane to the c axis (parallel to the polymer chain axis) for a stage-1 Cs-doped PPV sample.

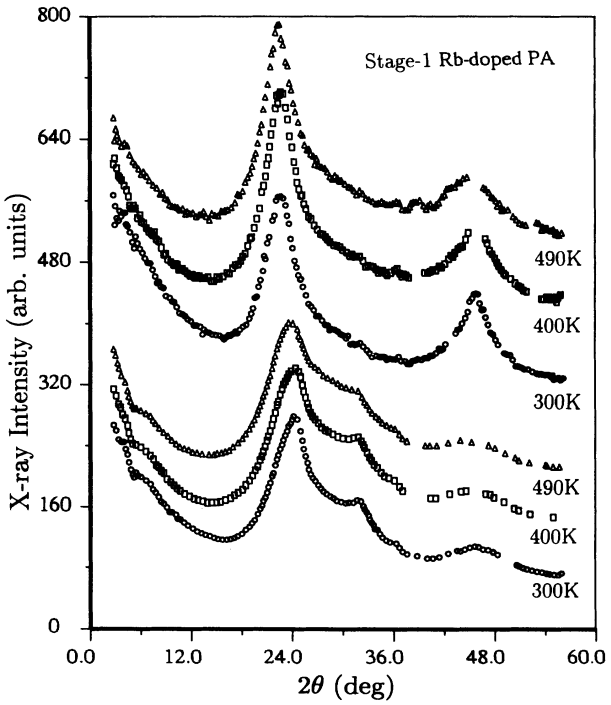

FIG. 8. Experimental data for a powder average of the nonequatorial scattering in a stage-1 Rb-doped PA sample (bottom three scans) and the individual meridional ($00l$) scans along the polymer chain axis (top three curves) at stated temperatures. Gaps in the plotted data result from the removal of sharp scattering artifacts (e.g., from Be windows).

shift to lower angles. This observed broadening arises solely from systematic changes in the intensity variations *along* the alkali-metal layer lines implying a gradual loss in the *interchannel* Rb^+-Rb^+ correlations. While the Rb-ion c-axis repeat increases to 3.99 Å at 490 K, there is no measurable change of the $l=1$ layer line radial width in the individual θ-2θ scans parallel to the polymer c axis (three scans at top in Fig. 8). Hence, increased temperature has a minimal effect on the intrachannel ordering. Equivalent scans of stage-1 K-doped PA- and Cs-doped PA by Leitner *et al.*[36] (at l_{N_2} temperatures) also do not manifest dramatic intrachannel ordering phenomena. In contrast to graphite intercalation compounds (GIC's) or other low-dimensional guest-host composites,[52] these stage-1 alkali-metal-doped polymers do not exhibit dramatic structural phase transformations at the temperatures that are accessible.

At elevated temperatures, there are systematic intensity variations between the two resolved rubidium layer lines indicating an increase in the thermally derived alkali-metal-ion displacements. A quantitative estimate of this displacement is an important input parameter for calculations which address the role of dopant-ion disorder in altering the transport characteristics.[53,54] Because of the complexity in the Rb^+-Rb^+ interchannel correlations, a direct comparison of relative layer line intensities or an introduction of an anisotropic temperature factor into a 3D structure-factor calculation are problematical. We have made an estimate of the intrachannel Rb-ion motions by averaging over the intensity modulations along the two resolved layer lines while including corrections for the Lorentz-polarization factor and for equatorial temperature effects. Comparison of the relative $l=1$ to $l=2$ layer line intensity ratios yields total static and dynamic alkali-metal axis root-mean-square displacements of ~0.2 Å at both 300 and at 400 K and approximately 0.3 Å at 490 K. Hence, the axial deviations from the equilibrium positions within 25-Å "domains" appear modest and are slightly less than the equatorial displacements. An analogous study[35] of unoriented stage-1 Cs-doped PA inferred somewhat stronger axial dopant-ion displacements.

The constant-intensity contour map for stage-1 Cs-doped PPV, shown in Fig. 7(b) also exhibits scattering from the $l=1$ and $l=2$ Cs^+-ion layer lines. For these compounds, an intrachannel spacing close to 4.5 Å is found, somewhat larger than that of the stage-1 alkali-metal-doped PA samples. Just two reflections can be clearly resolved along the $l=1$ layer line, indexed as the (101) and (111), with projected equatorial components of ~0.41 $Å^{-1}$ and ~0.92 $Å^{-1}$, respectively. These positions are best modeled using a base-centered orthorhombic unit cell, where only Cs ions in adjacent channels along the **a** direction are effectively staggered by $c_{Cs}/2$ [see Fig. 1(c)]. This unexpected alkali-metal organization may have its origin in the peculiar structural packing of the PPV host in which adjacent (100) planes of polymer chains exhibit substantial axial disorder.[29,55] However, the presence of an anomalously weak, but observable, (111) reflection suggests that some 3D interchannel correlations are still present in stage-1 Cs-PPV. We also note that the nonequatorial reflections of stage-1 Cs-doped PPV always exhibit a less pronounced angular arcing than those of stage-1 Rb-doped PA, which is indicative of poorer overall 3D ordering.

However, all stage-1 Cs-doped PPV samples exhibited one singular result with the appearance of comparatively narrow radial peak widths for the Cs $l=1$ layer line in scans parallel to the c axis. In general, Cs-PPV-doped samples exhibit intrachannel alkali-metal correlations lengths, ξ_{Cs}, of typically 70 Å. If similar ion-ion interactions always dominated the channel ordering process, then we would naively expect a ξ value close to those of alkali-metal-doped PA. These facts also suggest that strong host-guest interactions are the most significant factor in determining the actual channel structure. The leading edge of the $l=2$ layer line is somewhat broader, suggesting the presence of additional types of disorder.[47]

For the powder averaged nonequatorial scattering (the bottom two curves in Fig. 9) of stage-1 Cs-doped PPV, only the (101) reflection can be clearly resolved. Once again, there is a similar lack of dramatic thermally induced structural changes, with only a slight loss in the intrachannel Cs^+-Cs^+ correlations and no significant variations in the $l=1$ layer line radial widths (as determined by the leading edge) in scans parallel to the polymer chain axis (Fig. 9, two scans at top). Because the stage-1 PPV continues to slowly evolve, the shift to higher angle in the 540-K scan is only representative of an increase in the intrachannel Cs^+-ion density.

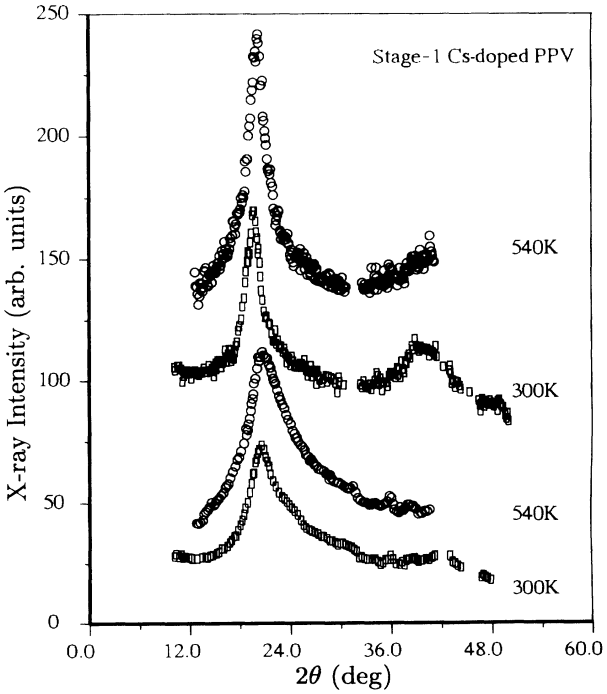

FIG. 9. Experimental data for a powder average of the nonequatorial scattering in a stage-1 Cs-doped PPV sample (bottom two scans) and the individual meridional (00l) scans (top two curves) at stated temperatures. Gaps in the plotted data result from the removal of sharp scattering artifacts (e.g., from Be windows).

V. DISCUSSION AND CONCLUSIONS

From analysis of both the equatorial and nonequatorial data we conclude that these polymer compounds experience significant interactions between the dopant ions and the surrounding polymer chains. In alkali-metal-doped graphite intercalation compounds (GIC's), the guest-host forces generate displacements of the alkali-metal ions towards the carbon hexagon centers as indicated by the appearance of modulation satellites in the x-ray-diffraction profiles. We find no evidence for the analogous behavior in these stage-1 polymer intercalation compounds. However, the c-axis modulation potential experienced by the dopant ions centered within polymer channels must be qualitatively different than the full graphite corrugation of GIC's (as seen in Fig. 10). Even for PPV, with its significant phenylene ring composition, the rotation of the polymer chains should modify the corrugation potential actually experienced.

Previous structural studies of alkali-metal-doped PA (Ref. 32) have invoked the existence of axially commensurate phases (along the c axis) whereby the channel size is determined by the minimum alkali-metal ion to carbon-atom spacing. Although commensurate spacings do occur at intermediate dopant levels,[14,32] the stage-1 "tetragonal" structures (as well as those of the hexagonal-phase structures) typically yield incommensurate alkali-metal-ion repeats. Thus, the projected minimum chain to ion spacing should be emphasized as the most significant parameter in determining the overall lateral dimensions. In Cs-doped PPV, the increased length of polymer major-axis projection (due to the presence of phenylene rings) allows for global chain rotation to bring the ions into closer proximity to the excess negative-charge resident in the p_z orbitals of the surrounding polymer chains. An additional advantage of the chain-axis rotation in the stage-1 Cs-doped PPV sample is an energetically favorable increase in the H-H spacing between neighboring chains. This 25° chain-axis rotation reduces the minimum chain to ion spacing by 0.3 Å to 3.1 Å, a distance ~0.1 Å less than the nominal 3.21 Å spacing of stage-1 Cs-doped PA, which is considered to be optimally spaced assuming a commensurate structure.[9] In comparison to low-stage Cs-GIC's,[56] in which the alkali-metal ions are located at (or near) carbon hexagon centers, the polymer spacing is expanded by only 0.1 Å (see Table II). Moreover, this distancing appears to be essentially temperature insensitive. To achieve such a close spacing, elastic deformation of the polymer chains about the dopant ion, through a combination of bond angle and torsional angle readjustments, seems probable. Since stage-1 alkali-PA compounds are also incommensurate, it is expected that they would undergo a similar deformation.

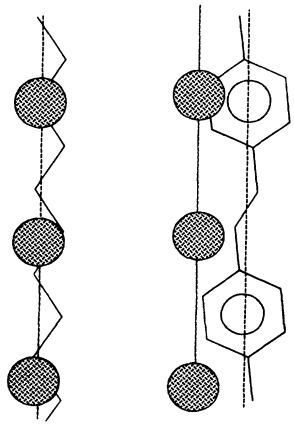

FIG. 10. Position of the alkali-metal ions in the channels relative to the host with the translational distortion of PA (left) and rotational motion of PPV (right).

For the smaller PA polymer host, there are a number of factors that appear contradictory. Because of the smaller 0.36-Å lateral carbon displacements from the chain-axis center in PA chains, simple chain-axis rotations of the undistorted high-symmetry stage-1 tetragonal structure, as shown in Fig 2(a), will not achieve as dramatic a reduction in the alkali-metal ion to carbon-atom spacings as in the stage-1 Cs-doped PPV compounds. The translational displacement, indicated by structure-factor calculations, neither increases nor decreases the channel to chain perpendicular spacing and effects only a slight decrease in the carbon atom to alkali-metal ion spacing. Furthermore, this motion also has the additional complication of bringing neighboring hydrogen atoms in adjacent polymer chains into closer proximity and thus, tends to increase the effective hydrogen repulsion.

Given that all structure evidence presented so far in this paper supports a claim of strong guest-host interactions with compensating polymer chain distortions, the simple translational displacements observed in PA could be an indirect consequence of more subtle structural rearrangements. One such possibility is that this average structure is actually representative of chain bond-angle changes and torsional twists about an axis that is displaced along the chain major axis as shown in Fig. 11. Thus, the PA chains may actually undergo a systematic sequence of twists that simultaneously reduce both the carbon-alkali-metal-ion distance and the repulsive hydrogen-hydrogen interaction. We note that neutron-scattering studies of stage-1 K-doped PA by Aimé *et al.*,[57] which are very sensitive to the chain orientation, required the existence of PA chain rotations. The only complication to the aforementioned structural scenario is that the linear arrays of alkali-metal ions would have only two polymer chains as nearest neighbors instead of four.

TABLE II. Various guest-host distances described in Fig. 6 for alkali-metal intercalated polymers and graphites (from Ref. 52).

Dopant	Stage-1 PA d spacing (Å)	Stage-1 PPV d spacing (Å)	Stage-1 GIC's d spacing (Å)
K	2.96		2.66
Rb	3.09		2.83
Cs	3.21	3.08	2.98

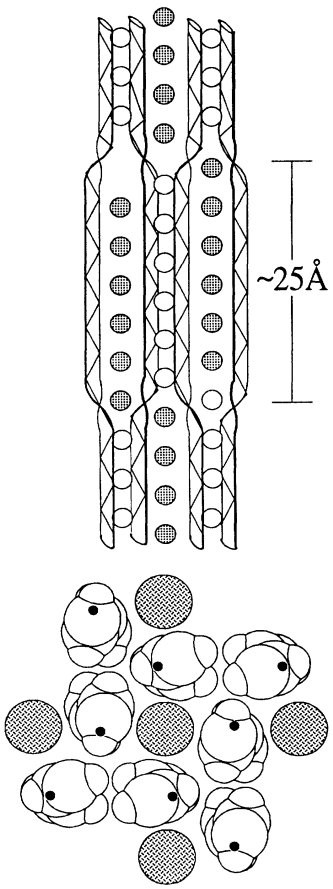

FIG. 11. Schematic views of alkali-metal-doped polyacetylene showing a possible sequence of polymer chain torsional distortions about an axis displaced from the chain centers (indicated by the small dots).

This circumstantial claim for PA chain distortions can also provide, in part, a tentative basis for interpreting the anomalously small intrachannel alkali-metal–alkali-metal correlation lengths observed in the PA compounds. We suggest that the reduced ξ's of the alkali-metal ions in stage-1 PA samples correspond to the axial spacing at which these distortions occur. An immediate consequence to these twists if they were to extend over only 3–4 (CH) units is that neighboring 25-Å domains would be identified with two distinct sets of nearest-neighbor polymer chains. Clearly, any distortions from PA planarity cost elastic energy but the gas-phase torsion potentials, as determined by Brédas and Heeger[58] for *undoped* acetylenic oligomers, suggest that small torsional displacements about a "single bond" are not energetically unfavorable.

There are at least three qualitative differences in PPV that may account for the enhanced correlation lengths observed in our Cs-doped PPV samples. First of all, the transferred charge will be distributed differently in PPV than in PA because of the greater number of carbons atoms per unit length. Hence, intrachannel alkali-metal–alkali-metal interactions may be more pronounced. Second, the repulsive vinyl-phenyl hydrogen interaction may allow for both stronger and more homogeneous local deviations from planarity between adjacent phenyl rings.[41] Finally, we note that there are fundamentally different charge excitations arising from the nondegenerate nature of the PPV charge excitations, thus the charge transferred to the backbone charge should exhibit a greater degree of localization than in polyacetylene.

In conclusion, we have investigated the structure and thermal response of two representative stage-1 alkali-metal-doped conjugated polymers. Although the relative guest-host size relationship seems to be responsible for the specific channel symmetry (threefold versus fourfold), the details of the local guest-host interactions are of central importance for determining the actual structural distortions experienced. Consequently, stage-1 Cs-doped PPV samples undergo chain-axis rotations while stage-1 alkali-metal-doped PA's exhibit a translational response. In either case, these fourfold channel structures exhibit only modest temperature variations. Since x-ray-diffraction studies are not sensitive to the location of the polymeric hydrogen, additional neutron-scattering experiments should provide further insight. Analogous studies of the threefold channel compounds are also likely to be very interesting for these systems experience much weaker alkali-metal–alkali-metal interchannel interactions.[31]

ACKNOWLEDGMENTS

The financial support by the University of Wisconsin and NSF DMR Grant No. DMR-8917530 (D.C. and M.J.W.), by the AFOSR (F.E.K.) and jointly by DARPA-AFOSR under AFOSR Contract No. F49620-88-C0138 (Y.C. and A.J.H.), is gratefully acknowledged. We also acknowledge John Fischer for illuminating discussions and helpful comments.

[1]S. Roth and H. Bleier, Adv. Phys. **36**, 385 (1987).
[2]A. J. Heeger, J. R. Schriefer, and W.-P. Su, Rev. Mod. Phys. **40**, 3439 (1988).
[3]W.-P. Su, Adv. Phys. **36**, 385 (1987).
[4]Han-Yong Choi, E. J. Mele, Jingfei Ma, and J. E. Fischer, Synth. Met. **27**, A75 (1988).
[5]H.-Y. Choi and E. J. Mele, Phys. Rev. B **40**, 3439 (1989).
[6]H.-Y. Choi, A. B. Harris, and E. J. Mele, Phys. Rev. B **40**, 3766 (1989).
[7]R. H. Baughman, L. W. Shacklette, N. S. Murthy, G. G. Miller, and R. L. Elsenbaumer, Mol. Cryst. Liq. Cryst. **118**, 253 (1985).
[8]R. H. Baughman, N. S. Murthy, G. G. Miller, and L. W. Shacklette, J. Chem. Phys. **79**, 1065 (1983).
[9]R. H. Baughman, N. S. Murthy, and G. G. Miller, J. Chem. Phys. **79**, 515 (1983).
[10]L. W. Shacklette and J. E. Toth, Phys. Rev. B **32**, 5892 (1985).
[11]M. J. Winokur, Y. B. Moon, A. J. Heeger, J. Barker, D. C. Bott, and H. Shirakawa, Phys. Rev. Lett. **35**, 2329 (1987).
[12]P. A. Heiney, J. E. Fischer, D. Djurado, J. Ma, D. Chen, M. J.

Winokur, N. Coustel, P. Bernier, and F. E. Karasz, Phys. Rev. B **44**, 2507 (1991).
[13]D. Djurado, J. E. Fischer, P. A. Heiney, J. Ma, N. Coustel, and P. Bernier, Synth. Met. **34**, 683 (1990).
[14]D. Billaud, F. Saldi, J. Ghanbaja, D. Begin, and M. LeLaurain, Synth. Met. **35**, 113 (1990).
[15]J. Ma, J. E. Fischer, C. Mathis, B. Francois, N. Coustel, and P. Bernier, Phys. Rev. B **44**, 11 609 (1991).
[16]J. Ma, J. E. Fischer, Y. Cao, and A. J. Heeger (unpublished).
[17]D. Chen, M. J. Winokur, and F. E. Karasz, Synth. Met. **41**, 341 (1991).
[18]H. A. Mizes and E. M. Conwell, Phys. Rev. B **43**, 9053 (1991).
[19]Y. B. Moon, Y. B. Moon, A. J. Heeger, J. Barker, and D. C. Bott, Macromolecules **20**, 2457 (1987).
[20]For example, see G. Wieners, R. Weizenhofer, M. Monkenbusch, M. Stamm, G. Lieser, V. Enkelmann, and G. Wegner, Makromol. Chem., Rapid Commun. **6**, 425 (1985).
[21]For a general review, see *Handbook of Conducting Polymers,* edited by T. Skotheim (Dekker, New York, 1986), Vols. 1 and 2.
[22]N. Basescu, Z.-X. Liu, D. Moses, A. J. Heeger, H. Naarmann, and N. Theophilou, Nature **327**, 403 (1987).
[23]J. Tsukamoto, A. Takahashi, and K. Kawasaki, Jpn. J. Appl. Phys. **29**, 125 (1990).
[24]M. A. Masse, R. J. Composto, R. A. L. Jones, and F. E. Karasz, Macromolecules **23**, 3675 (1990).
[25]D. B. Tanner, G. L. Doll, A. M. Rao, P. C. Eklund, G. A. Arbuckle, and A. G. MacDiarmid, Synth. Met. **28**, D141 (1989).
[26]Y. Nogami, H. Kaneko, H. Ito, T. Ishiguro, T. Sasaki, N. Toyota, A. Takahashi, and J. Tsukamoto, Phys. Rev. B **43**, 11 829 (1991), and references cited therein.
[27]H. Kume, S. Masubuchi, K. Mizoguchi, K. Mizuno, and H. Shirakawa, Synth. Met. **17**, 533 (1987).
[28]J. P. Pouget, P. Robin, R. Comes, H. W. Gibson, A. J. Epstein, and D. Billaud, Physica B+C **127B**, 158 (1984).
[29]T. Granier, E. L. Thomas, D. R. Gagnon, R. W. Lenz, Jr., and F. E. Karasz, J. Polym. Sci., Polym. Phys. Ed. **24**, 2793 (1986).
[30]N. S. Murthy, L. W. Shacklette, and R. H. Baughman, Phys. Rev. B **40**, 12 550 (1989).
[31]D. Chen, M. J. Winokur, M. Masse, and F. E. Karasz, Phys. Rev. B **41**, 6759 (1990).
[32]N. S. Murthy, L. W. Shacklette, and R. J. Baughman, J. Chem. Phys. **87**, 2346 (1987).
[33]F. Saldi, J. Ghanbaja, D. Begin, M. LeLaurain, and D. Billaud, C. R. Acad. Sci. **309**, 671 (1989).
[34]F. Saldi, D. Begin, and D. Billaud, Solid State Commun. **76**, 595 (1990).
[35]D. Djurado, J. E. Fischer, P. A. Heiney, and J. Ma, Phys. Rev. B **41**, 2971 (1990).
[36]O. Leitner, H. Kahlert, G. Leising, and J. Fink, Synth. Met. **28**, D225 (1989).
[37]D. R. Gagnon, J. D. Capistran, F. E. Karasz, R. W. Lenz, and S. Antoun, Polymer **28**, 567 (1987).
[38]J. M. Machado, F. E. Karasz, R. F. Kovar, J. M. Burnett, and M. A. Druy, New Polym. Mater. **1**, 189 (1989).
[39]Y. B. Moon, S. D. D. V. Rughooputh, A. J. Heeger, A. O. Patil, and F. Wudl, Synth. Met. **29**, E79 (1989).
[40]D. D. C. Bradley, R. H. Friend, T. Hartmann, E. A. Marseglia, M. M. Sokolowski, and P. D. Townsend, Synth. Met. **17**, 473 (1987).
[41]D. Chen, M. J. Winokur, M. A. Masse, and F. E. Karasz, Polymer (to be published).
[42]H. Shirakawa and S. Ikeda, J. Polym. Sci. **2**, 3 (1971).
[43]D. Chen, Ph.D. thesis, University of Wisconsin, 1991.
[44]D. Chen, M. J. Winokur, and F. E. Karasz (unpublished).
[45]C. Fite and P. Bernier, Phys. Rev. B **36**, 4574 (1987).
[46]R. L. Elsenbaumer, P. Delannoy, G. G. Miller, C. E. Forbes, N. S. Murthy, H. Eckhardt, and R. H. Baughman, Synth. Met. **11**, 251 (1985).
[47]R. Hosemann and S. N. Bagchi, *Direct Analysis of Diffraction by Matter* (North-Holland, Amsterdam, 1962).
[48]This uncertainty relates to the relative precision with respect to temperature changes; the actual accuracy is estimated to be $\pm 3°$.
[49]B. E. Warren, *X-ray Diffraction* (Addison-Wesley, Reading, MA, 1969).
[50]D. Billaud, F. Saldi, J. Ghanbaja, D. Begin, and M. LeLaurain, Synth. Met. **41**, 63 (1991).
[51]D. Billaud (private communication).
[52]*Interaction in Layered Materials,* edited by M. S. Dresselhaus (Plenum, New York, 1986).
[53]K. Harigaya, Y. Wada, and K. Fesser, Phys. Rev. Lett. **63**, 2401 (1989).
[54]Richard J. Cohen and Arnold J. Glick, Phys. Rev. B **42**, 7659 (1990).
[55]T. Granier, E. L. Thomas, and F. E. Karasz, J. Polym. Sci., Polym. Phys. Ed. **26**, 65 (1988).
[56]S. Y. Leung, C. Underhill, G. Dresselhaus, T. Krapchev, R. Ogilvie, and M. S. Dresselhaus, Solid State Commun. **32**, 635 (1979).
[57]J. P. Aimé, M. Bertault, P. Delannoy, R. L. Elsenbaumer, G. G. Miller, and M. Schott, J. Phys. (Paris) Lett. **46**, L379 (1985).
[58]J. L. Brédas and A. J. Heeger, Macromolecules **23**, 1150 (1990).

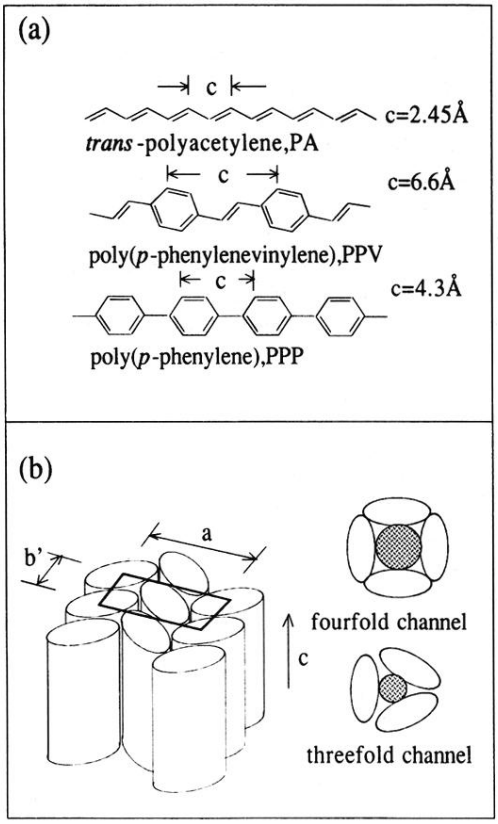

FIG. 1. (a) Projected *c*-axis structures of three prototypical conjugated polymers. (b) Packing of polymer chains when undoped (on left) and after alkali doping to threefold and fourfold channel structures.

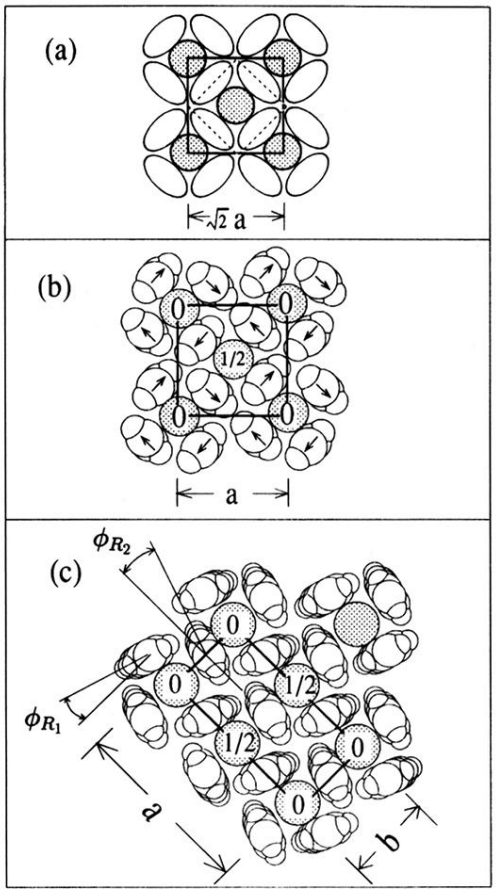

FIG. 2. Projected equatorial structure (perpendicular to the c axis) for (a) nominal $p4mm$ symmetry of stage-1 alkali-metal-doped polymers; (b) stage-1 alkali-metal-doped PA; (c) stage-1 Cs-doped PPV.

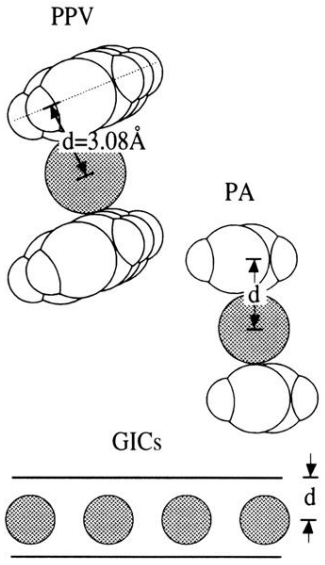

FIG. 6. Various guest-host spacings for Cs-doped PPV (on top), Rb-doped PA (middle), and stage-1 GIC (bottom) (Ref. 56) referred to in Table II and in the text.

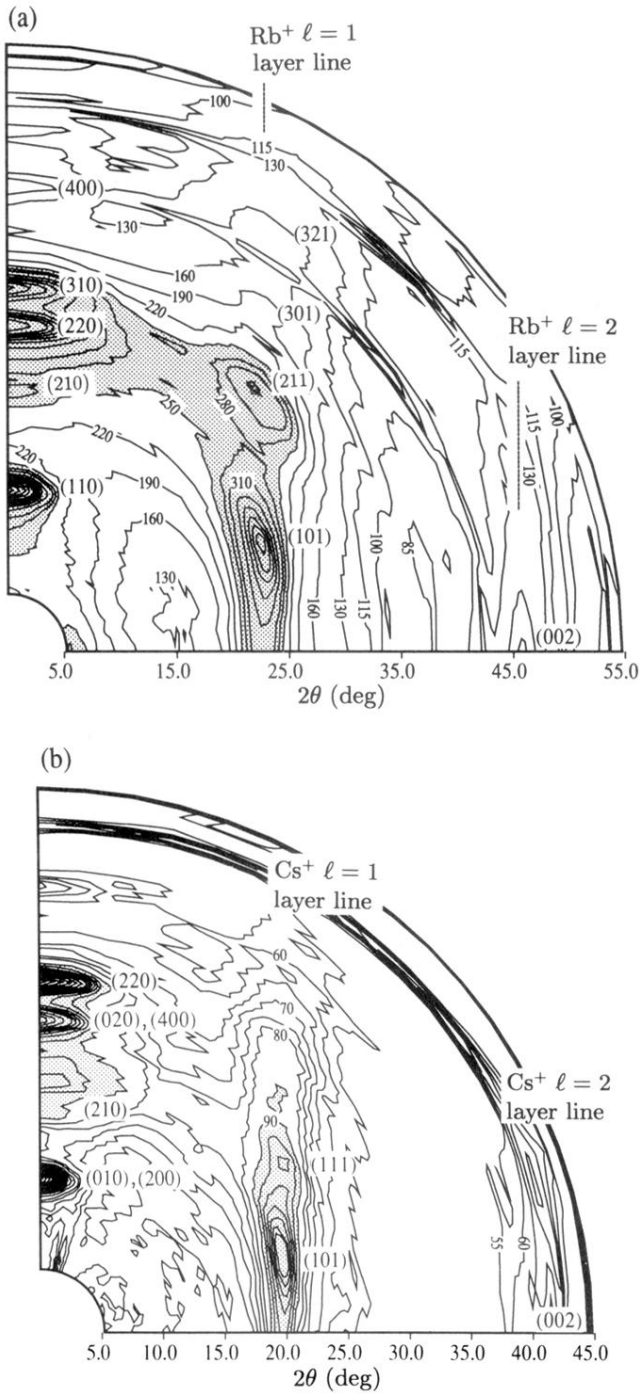

FIG. 7. (a) Map of the constant-scattering-density contours from the equatorial ($hk0$) plane to the c axis (parallel to the polymer chain axis) for a stage-1 Rb-doped PA sample. (b) Map of the constant-scattering-intensity contours from the equatorial ($hk0$) plane to the c axis (parallel to the polymer chain axis) for a stage-1 Cs-doped PPV sample.